Theor Chim Acta (1995) 91: 187–197

Theoretica Chimica Acta

Theoretical analysis of the electronic structure and reactivity of the CoP_3 core in [(triphos)CoP_3]

Alessandro Bencini, Massimo Di Vaira, Piero Stoppioni, Myriam G. Uytterhoeven
Università degli Studi di Firenze, Dipartimento di Chimica, Via Maragliano 75, I-50144 Firenze, Italia

Received May 9, 1994/Final revision received October 1, 1994/Accepted October 11, 1994

Summary. The electronic structure and reactivity of the compound [(triphos)-CoP_3] [triphos = 1, 1, 1-tris(diphenylphosphinomethyl)ethane] have been investigated using the semiempirical, extended Hückel (EH) approach, and density functional theory (DFT). The calculations have been performed on the model complex [$(PH_3)_3CoP_3$]. The orientation of the P_3 ring with respect to the (triphos)Co unit and electrophilic addition reactions have been investigated within the local density approximation (LDA). The staggered and eclipsed conformations of the P_3 group have been found to have comparable energies and the molecule is stabilized by a strong interaction within the *e* atomic orbitals (C_{3v} symmetry) mainly involving the $3p_z$ orbitals of phosphorus and $3d_{xz}$ and $3d_{yz}$ hybrid metal orbitals. Using H^+ as the electrophilic reagent four preferential sites of attack have been probed. The optimized structure of the most stable arrangement of the adduct corresponds to that experimentally observed in the monopositive cation [(triphos)CoP_3H]$^+$, which was obtained by protonation of the neutral species. The arrangements of two other favourable sites for the attack correspond to the geometries observed in the derivatives obtained by the electrophilic additions of CH_3^+ and, respectively, $HgCH_3^+$. The geometry of the model complex [$(PH_3)_3Co(P_3CH_3)$]$^+$ has been optimized using DFT–LDA and compared to that of [(triphos)$Co(P_3CH_3)$]$^+$.

Key words: Extended Hückel – Density functional theory – Local density approximation

1 Introduction

In recent years the reactivity of the P_3 group η^3-coordinated to metal centres in the presence of suitable stabilizing coligands has been investigated and found to be varied, depending on several factors [1, 2]. When involved in neutral complexes, the P_3 group predominantly acts as a Lewis base toward electrophiles such as metal carbonyl fragments [3] and the isolobal CH_3^+ cation [4], which bind to one phosphorus atom of the group completing a pseudo tetrahedral arrangement around it. When involved in cationic complexes, the P_3 ring undergoes insertion reactions and cleavage of a P–P bond by electron-rich metal–ligand fragments,

such as the bent $Pt(PPh_3)_2$ system [5]. In the latter reactions the ring is considered to behave as an acceptor via its antibonding orbitals. The $HgCH_3^+$ reactant plays an intermediate role toward neutral P_3 derivatives, as it binds in bridging position between two phosphorus atoms with a minor elongation of the P–P bond distance [6]. Finally, the electrophilic attack on the [(triphos)CoP_3] compound [triphos = 1, 1, 1-tris(diphenylphosphinomethyl)ethane] by the H^+ reactant, which may be considered isolobal to the previous systems endowed with an accessible empty σ orbital [essentially all of them, except $Pt(PPh_3)_2$], led to the $[(triphos)CoP_3H]^+$ species. The latter was assumed to contain the H atom in a bridging position between the metal and a phosphorus atom, in view of the distorted geometry of the CoP_3 moiety in the solid state [7].

We wish to report here the results of density functional theory (DFT) and extended Hückel (EH) calculations performed on a model system for the [(triphos)CoP_3] compound, where the tripod phosphine ligand was replaced by three properly oriented PH_3 groups. The possible directions for the electrophilic attack were probed by EH calculations and the binding mode previously proposed for H^+ [7] was tested by DFT calculations and compared with alternative arrangements. In the investigations of the reactivity of [(triphos)CoP_3] towards electrophiles the formalism developed by Weber et al. [8] based on EH calculations was employed, as it appeared to be particularly suitable to handling large organometallic complexes; the information from these calculations formed the starting point for quantitative DFT calculations. The structure of the methylated adduct has also been optimized.

2 Methods of calculation

Two types of MO calculations were performed: LCAO density functional calculations and EH-based reactivity calculations.

DFT calculations were performed using the Amsterdam Density Functional (ADF) program developed by Baerends et al. [9–11] in the local density approximation (LDA). The Vosko–Wilk–Nusair approximation for the exchange-correlation potential [12] was used throughout. The configuration $1s^2\,2s^2\,2p^6$ was treated as frozen core for cobalt. For phosphorus and carbon the $1s^2$ configuration was frozen. An uncontracted STO valence basis set was used consisting of: (1) a triple-ζ $1s$ and a $2p$ polarization function for hydrogen; (2) double-ζ $3s$ and $3p$, triple-ζ $3d$ and $4s$ and a single-ζ $4p$ for cobalt; (3) triple-ζ $3s$ and $3p$ and single-ζ $3d$ for phosphorus; (4) triple-ζ $2s$ and $2p$ and a single-ζ polarization $3d$ function for carbon. Expansion coefficients and orbital exponents are those provided by the program [9]. In the calculations the model complex $[(PH_3)_3CoP_3]$ was used, in which three PH_3 groups replaced the triphos ligand. A schematic view of the complex is shown in Fig. 1A where experimental and computed (see Sect. 3) distances are also indicated. Total energies were not computed directly, rather Ziegler's transition state method [13, 14] was applied. In this formalism the energy of the molecule is computed with respect to a reference state, formed by a sum of atomic or molecular fragments. In this way the energies obtained can be regarded as bonding energies. The bonding energy, ΔE, can be decomposed [14, 15] into chemically significant terms like steric interaction energy, ΔE^0, and electronic interaction energy, ΔE^T, according to

$$\Delta E = \Delta E^0 + \Delta E^T = \Delta E^0 + \sum_r \Delta E^r, \tag{1}$$

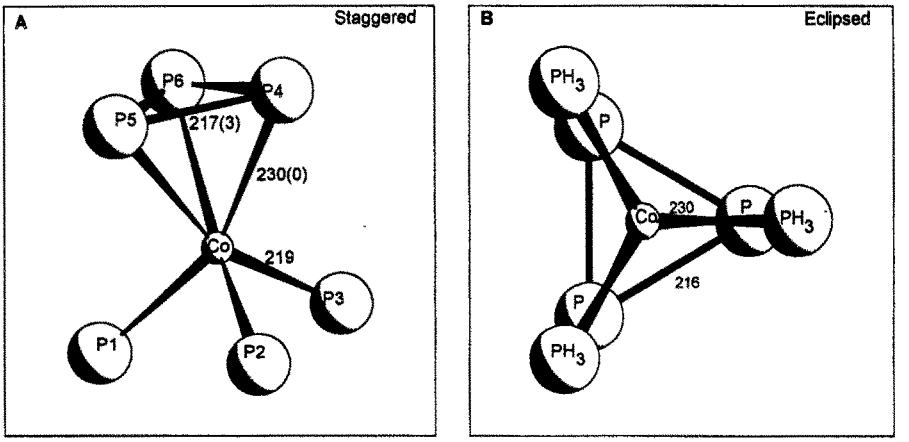

Fig. 1A, B. Sketch of the $[(PH_3)_3CoP_3]$ model system in the staggered conformation (**A**) and the eclipsed conformation (**B**); C_{3v} symmetry throughout. The P1–P3 labels refer to the phosphorus atoms of the PH_3 groups. Computed bond lengths (pm) are shown. The numbers in brackets correspond to the difference between calculated and experimental values, in that order

where ΔE^{Γ} is the contribution of the virtual orbitals in each symmetry representation Γ of the molecular point symmetry group to the electronic interaction energy. Geometry optimizations were performed using the Broyden–Fletcher–Goldfarb–Shanno algorithm [16].

The CACAO program package [17] was used to provide a simplified representation of the composition of the wave functions using single Slater atomic orbitals. This representation is more efficient than the usual way of representing the atomic wave functions using black and white lobes in order to show the atomic orbital composition of fragments. The extent of the interaction between fragments was always computed using DFT calculations.

EH-based reactivity calculations were done following the method described in Ref. [8] and using the program of calculation therein described. According to this method the reactivity of a substrate S in the presence of an electrophile R is described in terms of the S–R intermolecular interaction energy, E_{int}.

$$E_{int}(\boldsymbol{r}) = E_{es}(\boldsymbol{r}) + E_{ct}(\boldsymbol{r}), \tag{2}$$

where $\boldsymbol{r}$ represents the position of R with respect to the substrate; E_{es} represents the electrostatic energy contribution, which is the usual component included in the calculation of "MEPS", E_{ct} is the charge transfer energy represented by the difference between the total energy of the SR-molecule and the total energy of the separate S and R fragments. These energies were computed in the EH [18] framework as sums of the one-electron energies of the occupied orbitals times their respective occupation numbers. Several applications of the method have appeared in a review article [8]. The total energies were computed after reaching self-consistency in charge and configuration. The valence-state ionization energy H_{ii} of the reactant for the calculation of the E_{ct} component was chosen as E(HOMO) + 0.2 eV, i.e. − 7.74 eV.

3 Results and discussion

3.1 Orbital interactions

DFT calculations were performed on the model complex $[(PH_3)_3CoP_3]$ (Fig. 1) in which three PH_3 groups were introduced to mimic the triphos ligand. Calculations on the real complex are prohibitively long, and, to the best of our knowledge, they have never been attempted at any level of approximation. Complete geometrical optimization of the model complex was performed in C_{3v} symmetry and the computed bond distances and angles are: $Co–P_{PH3} = 216$ pm, $Co–P_{P3} = 229$ pm, $P_{P3}–P_{P3} = 216$ pm, $P_{PH3}–Co–P_{PH3} = 103°$, $P_{PH3}–Co–P_{P3} = 96°$ (the smallest of three such angles), $P_{P3}–Co–P_{P3} = 56°$. These figures compare favourably with the experimental values [19]: 219, 230, 214 pm, 92°, 104°, 55°. Discrepancies are found in the bond angles formed by the phosphine, which, in the real complex, are largely determined by ligand constraints. However, the substantial agreement in the $Co–P_{PH3}$ distances and the good fit of the experimental geometry of the CoP_3 moiety suggest that the bonding to the metal by the polyphosphine is sufficiently well reproduced, for the purposes of the present calculations, by the three PH_3 ligands. In all of the following calculations the geometry of the $(PH_3)_3Co$ fragment was frozen to that experimentally observed in the triphos complex, except when clearly indicated in the text.

DFT calculations on $[(PH_3)_3CoP_3]$ with the above geometrical constraint were performed for two different orientations of the P_3 fragment, staggered and eclipsed, depicted in Fig. 1A, B respectively. In the eclipsed arrangement the $Co–P_{P3}$ and $Co–P_{PH3}$ bonds lie in pairs on the symmetry planes, while in the staggered conformation they are rotated by 60° about the threefold axis, from the previous arrangement. Geometrical optimization of the two conformations in C_{3v} symmetry gave the bond distances shown in Fig. 1A, B. In Fig. 1A the computed distances for the CoP_3 core are also compared with the experimental data [19] and the agreement is found to be good. Incidentally, this is also indicative of scarce sensitivity of the CoP_3 dimensions to the choice made for the $P_{PH3}–Co–P_{PH3}$ angle, which, as stated above, was fixed at the experimental value and differed from that obtained with the preliminary, complete optimization. The eclipsed conformation was found to be only 4.6 kcal mol^{-1} higher in energy than the staggered one, in agreement with the fluctional behaviour in solution observed for the [(triphos)CoP_3] compound [20].

In order to rationalize the orbital interactions within the CoP_3 moiety, a fragment analysis of the molecular orbitals of $[(PH_3)_3CoP_3]$ in terms of those of the $(PH_3)_3Co$ and P_3 groups was undertaken. The valence energy levels computed for $[(PH_3)_3CoP_3]$ in the staggered conformation, labelled according to C_{3v} symmetry, are collected in Table 1 together with the net fragment population matrix. According to the net fragment populations, the orbitals can be classified as bonding, antibonding and nonbonding, the latter being those in which the charge is mainly localized on one of the two fragments. Bonding orbitals have a positive fragment overlap population value.

The HOMO of the $(PH_3)_3Co$ fragment is a triply occupied e antibonding orbital formed by ($3d_{xz}$, $3d_{yz}$) metal orbitals and sp phosphorus hybrids. At lower energy lie two essentially nonbonding metal orbitals: the ($3d_{x^2-y^2}$, $3d_{xy}$) e set and the a_1-type $3d_{z^2}$. Their composition is schematically shown in the Fig. 2A–C (left column), in the above order. The frontier orbitals of the P_3 fragment are linear combinations of the $3p$ orbitals of the phosphorus atoms, two of e-type and one of

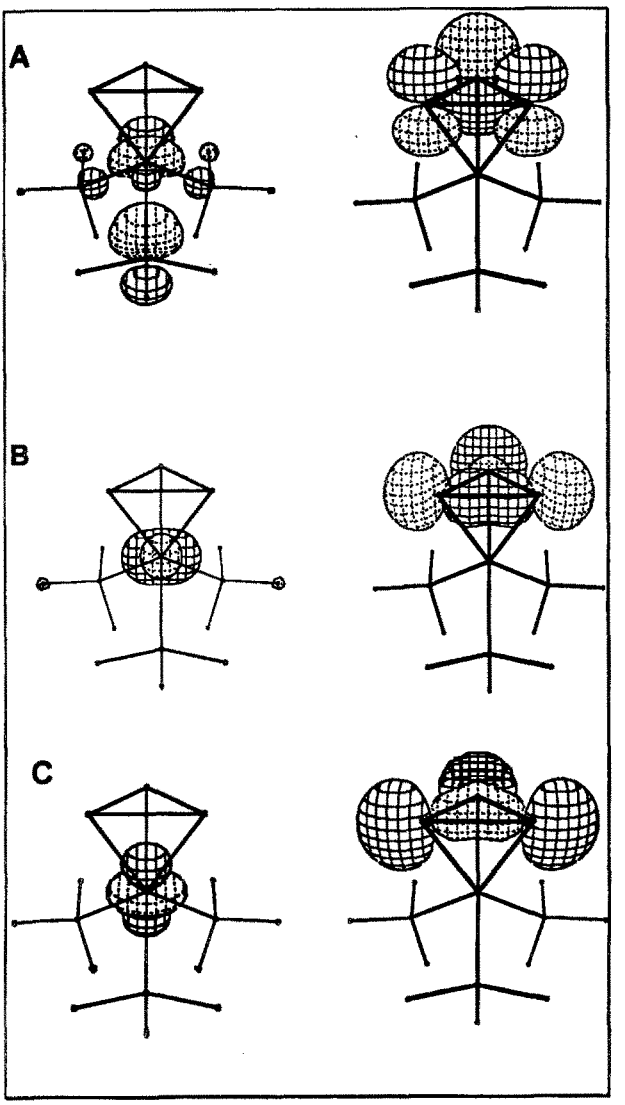

Fig. 2A–C. Schematic representations of frontier Molecular Orbitals of the fragments $(PH_3)_3Co$, left and P_3, right (see text). Only one component of each *e*-type MO is shown

a_1-type. The HOMO is a singly occupied *e* species formed by $3p_z$ orbitals (Fig. 2A, right; only one component shown). The other *e* set is a combination of the in-plane $3p_x$ and $3p_y$ orbitals (Fig. 2B, right). The totally symmetric linear combination of the $3p_x$ and $3p_y$ orbitals spans the a_1 irreducible representation (Fig. 2C, right) and forms the third frontier orbital of P_3.

From inspection of Table 1 the LUMO of $[(PH_3)_3CoP_3]$, $10a_1$, is seen to be a molecular orbital of the $(PH_3)_3Co$ fragment not interacting with those of the P_3 fragment. It has antibonding character between cobalt ($4s$ and $4p_z$) orbitals and those of the phosphines. The HOMO ($9e$) has slightly antibonding character between the two fragments. It is mainly composed of metal ($3d_{x^2-y^2}$, $3d_{xy}$) orbitals

Table 1. Valence energy levels and net fragment orbital populations[a] for $[(PH_3)_3CoP_3]$

Level		Energy (eV)	Fragment population		Overlap population
			$(PH_3)_3Co$	P_3	P_{ij}
$2a_2$		−0.42	.035	.938	.013
$12e$		−0.65	.550	.376	.036
$11e$		−1.23	.987	.012	0.
$11a_1$		−1.23	.973	.050	−.016
$10e$		−1.78	.569	.609	−.089
$10a_1$	LUMO	−1.88	1.00	.034	−.023
$9e$	HOMO	−4.53	.789	.266	−.028
$9a_1$		−4.79	.863	.175	−.019
$8e$		−4.84	.454	.442	.052
$7e$		−6.09	.249	.686	.032
$8a_1$		−6.65	.277	.783	−.030
$7a_1$		−7.36	.192	.839	−.015
$6e$		−7.47	.982	.012	.003
$6a_1$		−9.19	.724	.171	.052
$1a_2$		−10.20	1.00	0.	0.
$5e$		−10.29	.972	.036	0.
$4e$		−10.80	.991	.011	.003
$5a_1$		−11.41	.991	.004	.002
$3e$		−11.76	.050	.877	.003
$2e$		−16.54	1.00	0.	0.
$4a_1$		−17.13	.783	.200	.013
$3a_1$		−17.68	.223	.683	.047
$1e$		−60.22	1.00	0.	0.
$2a_1$		−60.61	1.00	0.	0.
$1a_1$		−94.78	1.00	0.	0.

[a] The orbitals are doubly occupied up to $9e$. For each molecular orbital the net fragment populations are in columns 3 and 4, the net fragment overlap populations in column 5.

Table 2. Decomposition[a] of the bonding energy of $[(PH_3)_3CoP_3]$ in the staggered and eclipsed conformations

Conformation	ΔE^0	ΔE^T			ΔE
		a_1	a_2	e	
Staggered	106.4	−14.5	0.0	−248.6	−155.6
Eclipsed	120.5	−15.9	0.0	−256.2	−151.0

[a] The bonding energy is defined in Eq. (1). All the values are in kcal mol^{-1}.

of the $(PH_3)_3Co$ fragment and the in-plane $3p_x$ and $3p_y$ orbitals of P_3. A combination of the same fragment orbitals, with bonding character, forms the $7e$ set. The a_1 combination of in-plane P_3 orbitals interacting with a mainly $3d_{z^2}$ orbital of $(PH_3)_3Co$ forms the $9a_1$ frontier orbital of the complex. The charge in the $9e$ and $9a_1$ orbitals is still mainly localized onto the $(PH_3)_3Co$ fragment. On the other hand, the $8e$ orbital, which is the highest-occupied with real bonding character, consists of a 50% combination of orbitals localized on the two fragments, exhibiting the largest electron delocalization. It is mainly formed by the HOMOs of

the two fragments, described in connection with Fig. 2A, which overlap strongly. The a_2 orbitals are nonbonding. It is apparent from the above considerations that the main bonding interactions between $(PH_3)_3Co$ and P_3 come from orbitals of *e*-type, the 8*e* being the most stabilizing.

Similar results were obtained for the $[(PH_3)_3CoP_3]$ complex in the eclipsed conformation, with minor changes in the energies of the a_1-type molecular orbitals. Somewhat larger variations were computed for the *e*-type molecular orbitals: the 9*e* orbital (HOMO) and the 7*e* are destabilized to -3.97 and -5.82 eV, respectively. The 8*e* is stabilized to -5.50 eV, whereas the other *e* orbitals are little affected.

Better insight into the electronic factors governing the relative stability of the $[(PH_3)_3CoP_3]$ complex in the two conformations is provided by the analysis of the contributions to the bonding energy, ΔE, shown in Eq. (1). According to the symmetry of the molecule, the electronic energy, ΔE^T, can be decomposed into contributions pertaining to the irreducible representations a_1, a_2, and *e*. The bonding energy decompositions for the staggered and eclipsed conformations are shown in Table 2. In both cases the largest orbital interaction arises from the *e* species and it is stabilizing (negative). The total orbital interaction energy is -263.1 kcal mol^{-1} for the staggered conformation and -272.1 kcal mol^{-1} for the eclipsed one. The orbital interactions actually favour the eclipsed conformation. The steric interaction, however, is larger (positive) for the eclipsed conformation and determines its lower total bonding energy. The steric interaction energy results from a calculation on the two separate fragments in which only the occupied orbitals on each fragment are included [13]. This energy can be further decomposed into ΔE_{el}, the electrostatic interactions between the fragments, and ΔE_{er}, the exchange repulsion between the fragments [14]. The above decomposition gives $\Delta E_{el} = -169.6$ kcal mol^{-1} and $\Delta E_{er} = 276.0$ kcal mol^{-1} for the staggered conformation, to be compared with the $\Delta E_{el} = -183.3$ kcal mol^{-1} and $\Delta E_{er} = 303.8$ kcal mol^{-1} values for the eclipsed one. The larger ΔE^0 value computed for the eclipsed conformation (Table 2) therefore arises from the electronic repulsion term ΔE_{er}, which is calculated to be larger than that of the staggered complex. In this framework, therefore, the relative stability of the two conformations is determined by the exchange repulsion energy which is lower in the staggered conformation. This conclusion should not be biased by the choice of the simplified model made to perform the calculations, as the difference in interfragment exchange repulsion energy for the two conformations should essentially originate from the interactions within the coordination sphere. The chains and phenyl groups of the triphos ligand, neglected in the model, lie farther apart and provide a rather uniform and flexible distribution which is not likely to favour one of the two conformations specifically.

Calculations were also performed to investigate the possible effects that changes in the angular parameters (*pyramidality*) of the $(PH_3)_3Co$ fragment might have on the dimensions of the CoP_3 pseudotetrahedron. These calculations were performed in the staggered conformation by varying the angle, ϕ, between the C_3 axis and the Co–PH_3 bond direction, from the experimental value of 56° and correspondingly optimizing the geometry of the CoP_3 group. Varying ϕ by $\pm 10°$ produces minor effects on the dimensions of the CoP_3 cage, the largest variations being 3 pm in the Co–P distances and 1 pm in the P–P bond lengths. This result was partly anticipated by the small differences detected between the fully optimized geometry and that with frozen P_{PH3}–Co–P_{PH3} angle, adopted in the calculations (see the discussion introducing Fig. 1). The bonding energies computed with respect to the free atoms for $\phi = 46°$, 56°, and 66° were -1675, -1697 and

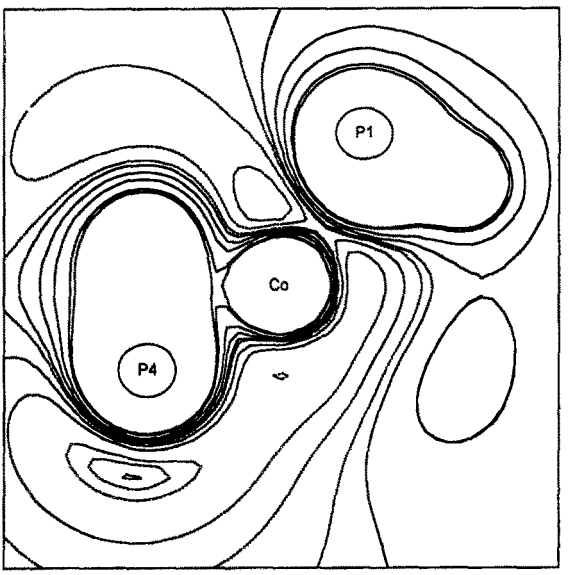

Fig. 3. Contour plot of E_{int} (see text). Broken lines mark the preferential zones to electrophilic attack

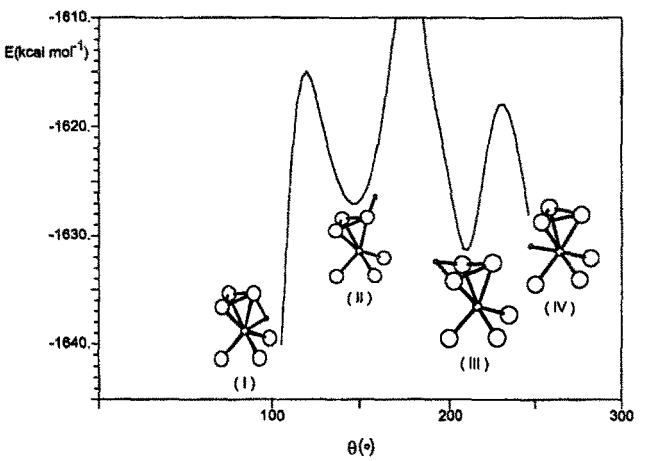

Fig. 4. Energy (kcal mol^{-1}) profile of the protonation of $[(PH_3)_3CoP_3]$. θ (°) is the angle between the C_3 axis of $[(PH_3)_3CoP_3]$ and the Co–H direction in the adduct

-1698 kcal mol^{-1}, respectively. Therefore, although the effects are small, as stated, ligands imposing particularly small values of the ϕ angle would be expected to destabilize the molecule.

3.2 Reactivity calculations

In order to investigate the possible sites of attack of the CoP_3 moiety by an electrophilic reagent, we performed EH-based reactivity calculations on the model complex of Fig. 1A. The electrophilic reagent was taken as the proton, H^+. The results of the calculations are shown in Fig. 3, where E_{int}, computed as in Eq. (2), is plotted in the P_1–Co–P_4 plane. The broken contours enclose regions of negative interaction energy, which indicate the preferential zones of attack by the electrophile H^+. A large region in which E_{int} is positive is placed all around the PH_3

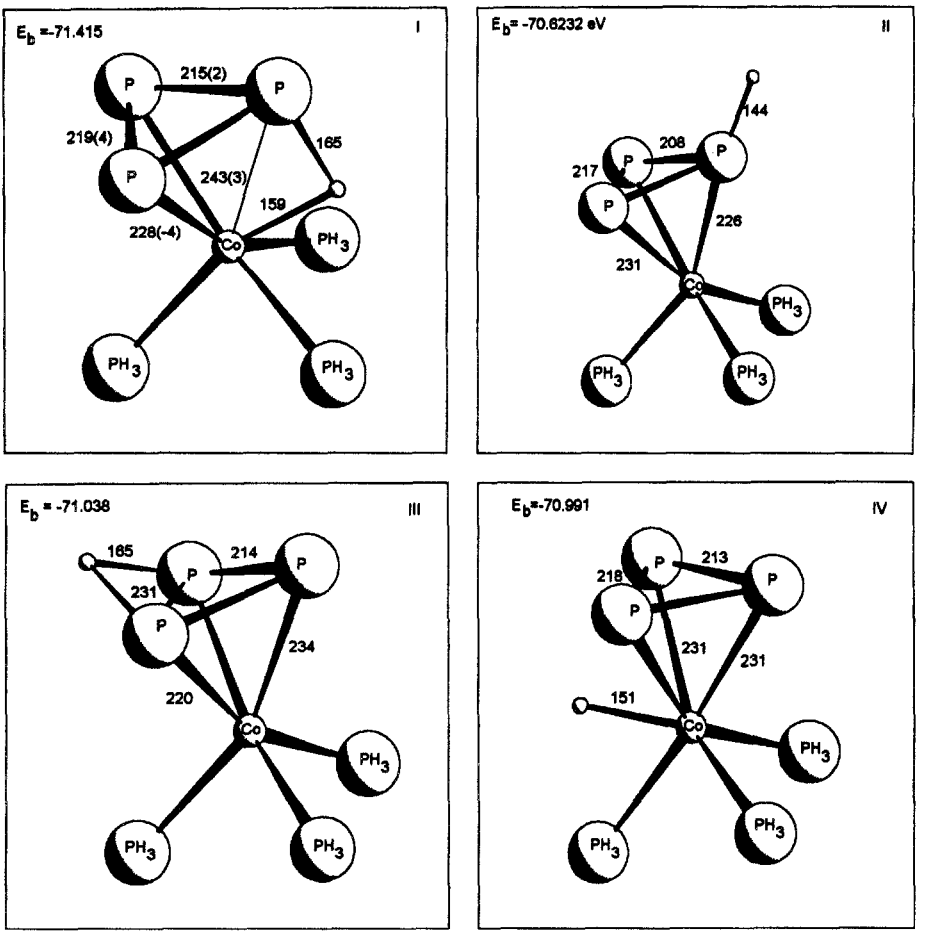

Fig. 5. DFT optimized geometries of the four conformations with minimal energy of the $[(PH_3)_3CoP_3] + H^+$ system. Computed bond lengths (pm) are also shown. The numbers in brackets correspond to the differences between the calculated and experimental vaues, the latter obtained for the $[(triphos)CoP_3H]^+$ complex

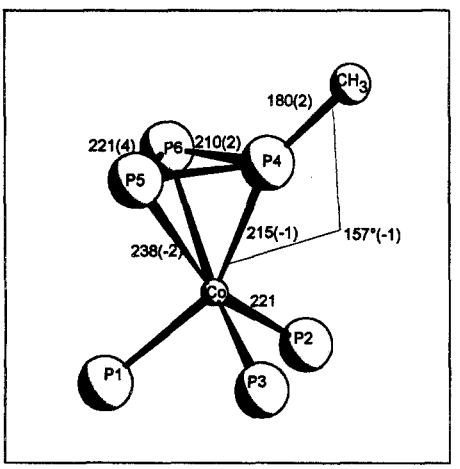

Fig. 6. DFT optimized geometry of the methylated complex $[(PH_3)_3Co(P_3CH_3)]^+$. Calculated bond lengths (pm) and bond angles (°) are also shown. P1–P3 refer to the phosphorus atoms of the PH_3 groups. The numbers in brackets are differences between calculated and experimental [4] values

groups, while a wide region of negative E_{int} values is computed around the P_3 ring. In the middle of the ring E_{int} is strongly positive. The minimum of E_{int} is computed near the cobalt nucleus. These results suggest that the electrophile can attack the complex in the region between Co and P_4 (Fig. 3) or, on the opposite side, in the region between the P_5–P_6 bond and the Co atom. All the regions of space in the vicinity of the centre of the P_3 ring should be unfavourable for the electophilic attack.

In order to verify whether different settings could be attained upon nucleophilic attack and to compare their relative stabilities, DFT calculations were performed on the model complex $[(PH_3)_3CoP_3H]^+$, assigning to the proton a set of positions in the P_1–Co–P_4 plane. In this set of calculations the geometry of $[(PH_3)_3CoP_3]$ was constrained to that obtained from the geometry optimization performed in C_{3v} symmetry (Fig. 1A), and only the position of the proton with respect to the complex was allowed to vary. The overall symmetry of the protonated complex was restricted to C_s. The results of the calculations are shown in Fig. 4 in the form energy vs. θ, where θ is the azimuthal angle yielding the orientation of H in the symmetry plane. Four conformations of minimal energy are clearly evident corresponding to the complexes denoted as I–IV. The absolute maximum is computed when the proton is on the perpendicular to the P_3 plane.

In order to fully compare the structures and the relative stabilities of the complexes I–IV, complete geometrical optimizations were performed on each of them in C_s symmetry. The optimized structures are shown in Fig. 5 together with the relevant computed geometrical parameters. The conformation having the absolute minimum bonding energy corresponds to the adduct I, where H forms a bridge between one of the phosphorus atoms of the P_3 ring and Co. The computed structure is also compared in Fig. 5 with the experimental one, from the crystal structure of $[(triphos)CoP_3H]^+$ [7]. The very good agreement obtained confirms that in $[(triphos)CoP_3H]^+$ the proton is in bridging position, as had been suggested [7]. Structure II resembles that found for the methylated derivative $[(triphos)Co(P_3CH_3)]^+$ [4], while a structure of type III was found [6] for the complex obtained by the electrophilic reaction of CH_3Hg^+ with $[(triphos)CoP_3]$.

In order to extend the study of the adducts of $[(triphos)CoP_3]$ and as a further test of the validity of the procedures, we have also performed a complete geometry optimization on the $[(PH_3)_3Co(P_3CH_3)]^+$ model of the methylated derivative, with the constraint of C_s symmetry. The minimized structure is compared with the experimental one in Fig. 6. The bonding of CH_3 to the P_3 group is well reproduced. As noted above, the CH_3^+ electrophile binds at a site corresponding to one of the relative minima detected for the H^+ attack. The possibility for CH_3^+ to attack along a Co–P edge, as for H^+ in the adduct I, was not investigated because such a position was considered to be hindered in the real molecule by the phenyl groups of the triphos ligand.

4 Conclusions

A semiempirical method, namely EH-based reactivity calculations, and DFT calculations have been combined to investigate the bonding and reactivity of the compound $[(triphos)CoP_3]$. The EH calculations provided a fast and efficient way to explore the regions around the molecule for possible sites of attack of nucleophilic reagents, while DFT calculations allowed a quantitative understanding of the orbital interaction mechanism and of the relative stabilities of the possible products of the reaction.

From the EH-based reactivity calculations a suitable direction for proton attack was suggested, grossly corresponding to the arrangement found for configuration II by the DFT approach. On the other hand, the DFT calculations have shown that I is in fact the most stable arrangement, in agreement with experiment. However, the two structures differ by only 18 kcal mol^{-1} (0.80 eV) and the arrangement of configuration II has actually been detected for the $[(PH_3)_3Co(P_3CH_3)]^+$ cation. Moreover, the small disagreement between the two approaches may be only apparent, since the best direction for attack may not strictly correspond to the most stable final arrangement. Interconversions between the different arrangements should be possible, because the protonated compound is known to be fluxional even at low temperatures in solution [7]. On the other hand, a thorough investigation of the possible interconversion paths by the DFT method was considered to be an excessively time-consuming task.

In conclusion, the geometry of the $[(PH_3)_3CoP_3]$ model for that of the [(triphos)CoP_3] complex and those of two products of electrophilic attack have been nicely reproduced by DFT calculation in the local density approximation. Using Ziegler's bonding energy decomposition scheme the relative stabilities of the staggered and eclipsed conformations of $[(PH_3)_3CoP_3]$ have been found to be mainly determined by the steric repulsions between the $(PH_3)_3Co$ and the P_3 fragments. We have found that the combined use of a fast computational technique such as the EH-based reactivity calculations, which allow to explore the reactivity of large organometallic moieties, and the more exacting DFT calculations can provide a satisfactory description of the reactivity and bonding of organometallic species at a reasonable expense of computer time.

Acknowledgements. Thanks are expressed to Prof. J. Weber and Dr. D. Stussi of the University of Geneva, who allowed us to use their programs for reactivity calculations. MGU acknowledges the EC *Human and Capital Mobility* Programme for research grant.

References

1. Di Vaira M, Sacconi L (1982) Angew Chem Int Ed Engl 21:330
2. Di Vaira M, Stoppioni P (1992) Coord Chem Rev 120:259
3. Midollini S, Orlandini A, Sacconi L (1979) Angew Chem Int Ed Engl 18:81
4. Capozzi G, Chiti L, Di Vaira M, Peruzzini M, Stoppioni P (1986) J Chem Soc Chem Comm 1799
5. Ref 2 and results to be published
6. Di Vaira M, Rovai D, Stoppioni P (1990) Polyhedron 9:2477
7. Di Vaira M, Stoppioni P, Midollini S, Laschi F, Zanello P (1991) Polyhedron 10:2123
8. Weber J, Stussi D, Fluekiger P, Morgantini P-Y, Kündig EP (1992) Comments Inorg Chem 14:27
9. ADF, release 1.0.2 (1993) Department of Theoretical Chemistry, Vrije Universiteit, Amsterdam
10. Baerends EJ, Ellis DE, Ros P (1973) Chem Phys 2:41
11. te Velde G, Baerends EJ (1992) J Comp Phys 99:84
12. Vosko SJ, Wilk L, Nusair M (1980) Can J Phys 58:1200
13. Ziegler T, Rauk A (1977) Theoret Chim Acta 46:1
14. Ziegler T, Rauk A (1979) Inorg Chem 18:1558
15. Bickelhaupt FM, Nibbering NMM, van Wezenbeek EM, Baerends EJ (1992) J Phys Chem 96:4864
16. Press WH, Flannery BP, Teukolsky SA, Vetterling WT (1989) Numerical Recipes. Cambridge University Press, Cambridge
17. Mealli C, Proserpio DM (1990) J Chem Education 67:399
18. Hoffman R, Fujimoto JR, Swenson C, Wan CC (1973) J Am Chem Soc 95:7644
19. Ghilardi CA, Midollini S, Orlandini A, Sacconi L (1980) Inorg Chem 19:301
20. Di Vaira M, Sacconi L, Stoppioni P (1983) J Organomet Chem 250:183